



Published in final edited form as:

Nature. ; 486(7402): 266–270. doi:10.1038/nature11114.

The deubiquitinase *USP9X* suppresses pancreatic ductal adenocarcinoma

Pedro A. Pérez-Mancera¹, Alistair G. Rust², Louise van der Weyden², Glen Kristiansen³, Allen Li⁴, Aaron L. Sarver⁵, Kevin A. T. Silverstein⁵, Robert Grützmann⁶, Daniela Aust⁷, Petra Rümmele⁸, Thomas Knösel⁹, Colin Herd², Derek L. Stemple², Ross Kettleborough², Jacqueline A. Brosnan⁴, Ang Li⁴, Richard Morgan⁴, Spencer Knight⁴, Jun Yu⁴, Shane Stegeman¹⁰, Lara S. Collier¹¹, Jelle J. ten Hoeve^{12,13}, Jeroen de Ridder¹², Alison P. Klein⁴, Michael Goggins⁴, Ralph H. Hruban⁴, David K. Chang^{14,15,16}, Andrew V. Biankin^{14,15,16}, Sean M. Grimmond¹⁷, APGI¹⁸, Lodewyk F. A. Wessels^{12,13,#}, Stephen A. Wood^{10,#}, Christine A. Iacobuzio-Donahue^{4,#}, Christian Pilarsky^{6,#}, David A. Largaespada^{19,#}, David J. Adams^{2,*}, and David A. Tuveson^{1,*}

¹Li Ka Shing Centre, Cambridge Research Institute, Cancer Research UK, and Department of Oncology, Robinson Way, Cambridge CB2 0RE, UK ²Experimental Cancer Genetics, Wellcome Trust Sanger Institute, Hinxton CB10 1SA, UK ³Institute of Pathology, University Hospital of Bonn, Sigmund-Freud-Str.25, 53127 Bonn, Germany ⁴Departments of Oncology and Pathology, The Sol Goldman Pancreatic Cancer Research Center, Sidney Cancer Center and Johns Hopkins University, Baltimore, MD 21287, USA ⁵Biostatistics and Bioinformatics Core, Masonic Cancer Center, University of Minnesota, 425 Delaware St SE MMC 806, Minneapolis, MN 55455, USA ⁶Department of Surgery, University Hospital Dresden, Fetscherstr. 74, 01307 Dresden, Germany ⁷Institute of Pathology, University Hospital Dresden, Fetscherstr. 74, 01307 Dresden, Germany ⁸Institute of Pathology, University Hospital of Regensburg, Franz-Josef-Strauss-Allee 11, 93053 Regensburg, Germany ⁹Institute of Pathology, University Hospital of Jena, Bachstraße 18, 07743 Jena Germany ¹⁰Eskitis Institute for Cell and Molecular Therapies, Griffith University, Nathan, Queensland, 4111, Australia ¹¹School of Pharmacy, University of Wisconsin, Madison, Wisconsin, 53705, USA ¹²Delft Bioinformatics Group, Department of EEMCS, Delft University of Technology, 2628 CD Delft, The Netherlands ¹³Bioinformatics and Statistics, The Netherlands Cancer Institute, Plesmanlaan 121, 1066 CX Amsterdam, The Netherlands ¹⁴The Kinghorn

Users may view, print, copy, download and text and data-mine the content in such documents, for the purposes of academic research, subject always to the full Conditions of use: http://www.nature.com/authors/editorial_policies/license.html#terms

*Correspondence to: da1@sanger.ac.uk; david.tuveson@cancer.org.uk.

#Equal contributions

Contributions: PAP-M performed the majority of all experiments, designed experiments, analyzed data, and wrote the manuscript. LvdW and JAB performed in vitro experiments. SS and SAW generated the conditional *Usp9x* mouse. LSC provided the CAGGS-SB10 and T2/Onc mice. AGR, ALS, KATS, JtH, JdR and LFAW conducted the CIS data analysis. GK, RG, DA, PR, TK and CP generated data from resected pancreatic tumors. AL, RHH, RM, SK, JY, AL, AL, MG and CAI-D analyzed human samples from autopsy series, and analyzed mouse pathology and methylation studies. CH, DLS and RK sequenced PDA human samples from autopsy series. APK provided statistical analyses for the human PDA data sets. APGI, DKC, SMG and AVB generated and analysed data from ICGC (for APGI full list of contributors see <http://www.pancreaticcancer.net.au/apgi/collaborators>). DAL provided the CAGGS-SB10 and T2/Onc mice, and analyzed data. DJA and DAT designed the study, analyzed the data, and wrote the manuscript. All authors commented upon and edited the final manuscript.

Competing financial interests

The authors declare no competing financial interests.

Cancer Centre, Cancer Research Program, Garvan Institute of Medical Research, 372 Victoria St, Darlinghurst, Sydney, NSW 2010, Australia ¹⁵Department of Surgery, Bankstown Hospital, Eldridge Road, Bankstown, Sydney, NSW 2200, Australia ¹⁶South Western Sydney Clinical School, Faculty of Medicine, University of NSW, Liverpool NSW 2170, Australia ¹⁷Queensland Centre for Medical Genomics, Institute for Molecular Bioscience, University of Queensland, St Lucia, Brisbane, QLD, Australia ¹⁸Australian Pancreatic Cancer Genome Initiative, The Kinghorn Cancer Centre, 372 Victoria St, Darlinghurst, Sydney, NSW 2010, Australia ¹⁹Masonic Cancer Center, University of Minnesota, Minneapolis, Minnesota 55455, USA

Abstract

Pancreatic ductal adenocarcinoma (PDA) remains a lethal malignancy despite tremendous progress in its molecular characterization. Indeed, PDA tumors harbor four signature somatic mutations¹⁻⁴, and a plethora of lower frequency genetic events of uncertain significance⁵. Here, we used *Sleeping Beauty* (*SB*) transposon-mediated insertional mutagenesis^{6,7} in a mouse model of pancreatic ductal preneoplasia⁸ to identify genes that cooperate with oncogenic *Kras*^{G12D} to accelerate tumorigenesis and promote progression. Our screen revealed new candidates and confirmed the importance of many genes and pathways previously implicated in human PDA. Interestingly, the most commonly mutated gene was the X-linked deubiquitinase *Usp9x*, which was inactivated in over 50% of the tumors. Although prior work had attributed a pro-survival role to *USP9X* in human neoplasia⁹, we found instead that loss of *Usp9x* enhances transformation and protects pancreatic cancer cells from anoikis. Clinically, low *USP9X* protein and mRNA expression in PDA correlates with poor survival following surgery, and *USP9X* levels are inversely associated with metastatic burden in advanced disease. Furthermore, chromatin modulation with trichostatin A or 5-aza-2'-deoxycytidine elevates *USP9X* expression in human PDA cell lines to suggest a clinical approach for certain patients. The conditional deletion of *Usp9x* cooperated with *Kras*^{G12D} to rapidly accelerate pancreatic tumorigenesis in mice, validating their genetic interaction. Therefore, we propose *USP9X* as a major new tumor suppressor gene with prognostic and therapeutic relevance in PDA.

The biological sequelae of PDA has been partially attributed to frequent and well characterized mutations in *KRAS* (>90%), *CDKN2A* (>90%), *TP53* (70%) and *SMAD4* (55%)¹⁻⁴. Recent genome-wide analyses have uncovered numerous additional somatic genetic alterations, although the functional relevance of most remains uncertain⁵. To explore the molecular genesis of PDA we previously generated a mouse model of Pancreatic Intraepithelial Neoplasia (mPanIN) by conditionally expressing an endogenous *Kras*^{G12D} allele in the developing pancreas⁸. Mice with mPanIN spontaneously progress to mouse PDA (mPDA) after a long and variable latency, providing an opportunity to characterize genes that cooperate with *Kras*^{G12D} to promote early mPDA. We hypothesized that such genes could be directly identified by applying insertional mutagenesis strategies^{6,7,10,11} in our mPanIN model, and that these candidates could represent “drivers” of PDA development.

Accordingly, we interbred our mPanIN model with two distinct *Sleeping Beauty* (SB) transposon systems and monitored mice for early disease progression. Our initial approach utilized the well characterized *CAGGS-SB10* transgenic allele to promote transposition⁶. Although *CAGGS-SB10* promoted PDA, a variety of non-pancreatic neoplasms and a paucity of identified Common Insertion Sites (CISs) in the recovered pancreatic neoplasms precluded a comprehensive analysis, potentially reflecting the variegated expression of *CAGGS-SB10*¹² (Supplementary Figures 1a and 2; Supplementary Tables 1 and 3b).

To increase the specificity and potency of SB mutagenesis, we generated a conditional *SB13* mutant mouse by targeting the *Rosa26* locus in embryonic stem cells (Supplementary Fig. 3a, b). The pancreatic specific expression and function of the conditional *SB13* allele was confirmed (Supplementary Fig. 3c), and we found that *SB13*-induced transposition by itself did not promote lethality or pancreatic tumorigenesis (Fig. 1a, Supplementary Fig. 4a). In contrast, KCTSB13 mice (*Kras^{LSL-G12D}; Pdx1-cre; T2/Onc; Rosa26-LSL-SB13*) rapidly progressed and succumbed to invasive pancreatic neoplasms (Fig. 1a–c). A cohort of 117 KCTSB13 mice (Supplementary Fig. 1b) was monitored for tumor development, and 103 of these mice were available for full necropsy and tissue procurement. The majority of such mice harbored multi-focal pancreatic tumors, and 198 distinct primary tumors and metastases were subjected to histological and molecular analysis. Most mice had invasive carcinomas (66/103) that consisted of classical mPDA (78.8%) or invasive cystic neoplasms (21.2%); 34.8% of mice also contained metastases predominantly in their liver and lungs (Supplementary Fig. 4c). The remainder of the mice (37/103) had preinvasive pancreatic tumors consisting of high grade mPanIN and cyst-forming papillary neoplasms (Supplementary Fig. 4b).

The candidate genes identified from the SB13 screen represented unanticipated candidates as well as many genes and pathways previously implicated in human PDA (Table 1, Supplementary Tables 2, 3a and 4). Indeed, various members of the TGF β pathway, including *Smad3*, *Smad4*, *Tgfr1* and *Tgfr2*, were collectively mutated in 32% of the tumors. Also, the Rb/p16Ink4a pathway was disrupted in 21% of the tumors. CISs representing the orthologues of additional human PDA genes included *Fbxw7* (24.2%), *Arid1a* (19.1%), *Acvr1b* (19%), *Stk11/Lkb1* (6.5%), *Mll3* (6%), *Smarca4* (6%) and *Pbrm1* (4.5%)^{5,13–15}. *Trp53* was the only commonly mutated PDA gene conspicuously absent, although the p53 regulatory deubiquitinase *Usp7* was a CIS (6.5%)¹⁶. Several CISs previously noted in insertional mutagenesis screens for hepatocellular carcinoma or gastrointestinal tract adenomas, but not typically mutated in PDA, were also identified in this study, including *Zbtb20*, *Nfib* and *Ube2h* in liver tumors¹⁰; and *Pten*, *Tcf12*, *Ppp1r12a*, and *Ankrd11* in gastrointestinal tract adenoma/adenocarcinoma¹¹. This indicates that many tumor progression pathways may be common to pancreatic, liver and gastrointestinal/colorectal tumors.

Unexpectedly, the most frequent CIS observed was the X-linked deubiquitinase *Usp9x*, a gene that had not been previously associated with PDA or other types of carcinoma in humans or mouse models. Indeed, the COSMIC data base revealed only one *USP9X* mutation in a case of ovarian cancer, although the functional relevance of this mutation has not been characterized (COSMIC mutation ID: 73237). *Usp9x* was disrupted in over 50% of

all tumors, with 341 insertions noted in the 101 tumors harboring this CIS (Fig. 1d, Table 1). Furthermore, *Usp9x* was also identified as a CIS in 4 samples from the initial SB10 screen (Supplementary Table 1), supporting its candidacy as a PDA genetic determinant. We confirmed that *Usp9x* was disrupted in tumors by isolating chimeric fusion mRNAs that spliced the *Usp9x* transcript to the T2/Onc transposon (Fig. 1e). In addition, the Usp9x protein was specifically absent in neoplastic cells in pancreatic tumors bearing intragenic insertions (Fig. 1f, g).

To characterize the cellular and molecular pathways affected by *Usp9x* in PDA, RNAi was used to deplete *Usp9x* in mPDA cell lines (Supplementary Fig. 5a). While Usp9x depletion did not affect the proliferation of monolayer cultures (Supplementary Fig. 5b), it significantly increased colony formation in soft agar (Fig. 2a, Supplementary Fig. 5c), compared to cells transfected with scrambled shRNAs. Additionally, *Usp9x* knock-down potently suppressed anoikis in mPDA cells (Fig. 2b). These properties of Usp9x were predominantly dependent upon its intrinsic deubiquitinase activity (Supplementary Fig. 6a, b).

Since USP9X was previously reported to positively regulate SMAD4 transcriptional activity¹⁷ and *SMAD4* is commonly mutated in PDA⁴, we hypothesized that *Usp9x* loss would attenuate Smad4 function or TGF β responsiveness in PDA cell lines. However, irrespective of Usp9x expression level, mPDA cell lines expressed Smad4 and were equally sensitive to p21 induction, growth inhibition and morphological alterations following exposure to TGF- β 1 (Supplementary Fig. 7a–d). Therefore we were unable to ascribe a specific role to Usp9x in the regulation of the Smad4/TGF β pathway in mPDA cells or tumors.

We next investigated several additional proteins reported to be regulated by Usp9x and involved in pathways relevant to cellular transformation. Although USP9X was previously shown to bind to and regulate two proteins involved in cell survival, ASK1¹⁸ and MCL1^{9,19}, we could not detect obvious changes in Ask1 or Mcl1 protein levels upon *Usp9x* loss (Fig. 2c). Usp9x has also been reported to deubiquitinate and thereby stabilize the E3 ligase Itch²⁰, decreased protein levels of Itch were observed in mouse and human PDA cells upon the depletion of Usp9x (Fig. 2c, Supplementary Fig. 8a). Importantly, ectopic Itch expression was sufficient to promote anoikis in mPDA cells (Fig. 2d), and Itch was partially responsible for the ability of Usp9x to promote anoikis and suppress colony formation (Supplementary Fig. 6c, d). Since Itch is known to promote the degradation of several proteins relevant to cell proliferation and survival²¹, we evaluated the protein expression of likely candidates including c-Jun, p63 and c-FLIP but observed no alterations (Supplementary Fig. 8b). Furthermore, the *Itch* gene was identified as a CIS in 13% of cases (Supplementary Table 2). Therefore, Usp9x mutation may promote tumorigenesis in part by disabling Itch function, and the Usp9x/Itch pathway may work to constrain pancreatic tumorigenesis.

To determine whether *USP9X* expression is aberrant in human PDA, three distinct patient cohorts were assessed. First, we analyzed a cohort of 100 Australian patients who underwent surgery for localized PDA and had detailed information available concerning clinical-

pathological characteristics and outcome (Supplementary Fig. 9, Supplementary Tables 5, 6). Tumor DNA from 88 patients in this cohort failed to yield somatic mutations in *USP9X*, consistent with prior reports⁵ (data not shown). Importantly, the low expression of *USP9X* mRNA correlated with poor survival following surgery ($p=0.0076$) (Fig. 3a), and multivariate analysis revealed that *USP9X* expression was an independent poor prognostic factor following surgery (Supplementary Table 7). We next analyzed autopsy specimens from a separate cohort of 42 American patients to determine that *USP9X* protein expression inversely correlated with a widespread metastatic pattern ($p=0.0212$) (Fig. 3b), and bore no relation to *SMAD4* expression (Supplementary Table 8). A third collection of PDA specimens obtained from resected German patients ($n=404$) were used to determine that *USP9X* and *ITCH* protein levels were decreased (Supplementary Fig. 10a, b) and concordant (Spearman-Rho correlation: 0.47; $p<0.01$) (Supplementary Table 9a) in tumors compared to normal pancreatic tissue. Additionally, the proportion of tumors that had undetectable *USP9X* (13.6%) or *ITCH* (30.5%) protein correlated with a worse outcome (Supplementary Fig. 11, Supplementary Table 9b, c), particularly regarding *USP9X* in the subset of high grade tumors (Fig. 3c, Supplementary Tables 10 and 11). Collectively, these findings implicate the loss of *USP9X* expression as a relevant event in human pancreatic cancer progression.

We found that *USP9X* was expressed throughout murine and human tumor development and lost focally in PDAs (Supplementary Figures 12, 13). Additionally, human PDA cell lines expressed lower levels of *USP9X* compared to non-PDA cancer cell lines (Supplementary Fig. 14). To investigate additional potential mechanisms of *USP9X* regulation in PDA, human cell lines were treated with the DNA methylase inhibitor 5-Aza-2'-deoxycytidine and the HDAC inhibitor trichostatin A. Both inhibitors modestly increased the *USP9X* mRNA and protein levels in most cell lines, suggesting that *USP9X* may be epigenetically silenced *in vivo* (Fig. 3d and Supplementary Fig. 15). Furthermore, although the promoter region of *USP9X* was not heavily methylated in tumor samples or PDA cells harboring low protein expression (data not shown), treatment with 5-Aza-2'-deoxycytidine did decrease colony formation of human PDA cells and this was partially reversed by concomitantly knocking-down *USP9X* (Supplementary Fig. 16).

To confirm that *Kras*^{G12D} cooperated with *Usp9x* loss to promote pancreatic cancer, a conditional *Usp9x*^{fl} allele was generated (Supplementary Fig. 17a) and interbred with *Kras*^{LSL-G12D}; *Pdx1-cre* mice to evaluate the impact on mPanIN progression. The mosaic expression of *Usp9x* in pancreas from *Pdx1-cre*; *Usp9x*^{fl/y} mice was confirmed by immunohistochemistry (Supplementary Fig. 17b). We found that all hemizygous male mice and heterozygous female mice carriers of the *Usp9x*^{fl} allele in the background of *Kras*^{LSL-G12D}; *Pdx1-cre* rapidly developed advanced mPanIN and microinvasive neoplasms within 3 months of age (Fig. 3e–f, Supplementary Fig. 18). Immunohistochemical analysis of mPanINs from heterozygous female mice demonstrated absence of *Usp9x* expression in the preneoplastic and neoplastic cells (Supplementary Fig. 18), implicating additional events such as X inactivation of the other locus in female mice^{22,23}. mPanINs in *Kras*^{LSL-G12D}; *Pdx1-cre*; *Usp9x*^{fl} mice expressed intranuclear Smad4, similar to *Kras*^{LSL-G12D}; *Pdx1-cre* mice (Supplementary Fig. 19a). Additionally, early passage pancreatic cell cultures prepared

from these mice confirmed the absence of the Usp9x protein and altered regulation of Itch (Supplementary Fig. 19b). Although some mice died of local or metastatic pancreatic cancer, aggressive oral papillomas often required the culling of young mice and demonstrated that *Kras*^{G12D} and *Usp9x* loss also cooperated to transform keratinocytes (Supplementary Fig. 19c).

Although a recent report implicated *USP9X* as a pro-survival gene by stabilizing MCL1⁹, potential inhibitors of *USP9X* should be developed with caution since we find that *Usp9x* has tissue specific effects including a tumor suppressor role in oncogenic *Kras*-initiated pancreatic carcinoma. *USP9X* is likely epigenetically silenced in a subset of PDA, thus explaining why prior DNA sequencing efforts have failed to identify this as participant in carcinogenesis, and offering the possibility that clinically available epigenome modulators may be useful agents to investigate in such patients. *ITCH* is a likely mediator of pancreatic tumor suppression by *USP9X*, and continued investigation of the *USP9X/ITCH* pathway is warranted. More generally, the identification of *Usp9x* through the use of transposon mutagenesis reaffirms the utility of *in vivo* mouse cancer screens to complement the direct investigation of human cancer.

Methods Summary

Kras^{LSL-G12D}(K)²⁴, *Pdx1-Cre*⁸ (C), *T2/Onc*⁶ (T), *CAGGS-SB10*⁶ (SB10) and *Rosa26-LSL-SB13* (SB13) strains were interbred to generate *Kras*^{LSL-G12D}; *Pdx1-Cre* (KC), *Kras*^{LSL-G12D}; *Pdx1-Cre*; *T2/Onc*; *CAGGS-SB10* (KCTSB10) and *Kras*^{LSL-G12D}; *Pdx1-Cre*; *T2/Onc*; *Rosa26-LSL-SB13* (KCTSB13) compound mutant mice. Non-quadruple mutant mice represented the comparison cohorts. *Kras*^{LSL-G12D} and *Pdx1-Cre* mice were interbred with *Usp9x*^{fl} mice to generate the *Kras*^{LSL-G12D}; *Pdx1-Cre*; *Usp9x*^{fl/+} and *Kras*^{LSL-G12D}; *Pdx1-Cre*; *Usp9x*^{fl/y} (KCU) compound mutant mice, as well as the two control cohorts *Pdx1-cre*; *Usp9x*^{fl/y} (CU) and *Kras*^{LSL-G12D}; *Pdx1-cre* (KC). *Usp9x*^{fl} mice were generated by Ozgene Pty. Ltd (Bentley, Australia). Mice were maintained in compliance with the UK home office regulations. Splinkerette PCRs were performed as described previously^{25,26}. Reads from sequenced tumors were mapped to the mouse genome assembly NCBI m37 and merged together to identify SB insertion sites, as previously described²⁵. Redundant sequences, as well as insertions in the *En2* gene and in the *T2/Onc* donor concatemer resident chromosome (chromosome 1), were removed. Mouse survival curves and cell culture experiments were analyzed with the GraphPad prism program. The IHC histoscore from the TMA samples and Kaplan-Meier survival curves were analyzed with SPSS18, and the Spearman-Rho correlation coefficient (2-sided) between *USP9X* and *ITCH* was calculated. The IHC *USP9X* histoscore and analysis was conducted using the Fishers Exact Test on post-mortem samples. The GEO accession number for the ICGC-APGI gene expression data is GSE36924.

Methods

Generation of *Rosa26-LSL-SB13* knockin mice

TL1 ES cells²⁷ were electroporated with linearized pRosa26-LSL-SA-SB13-BGHpolyA targeting construct and correctly targeted puromycin-resistant clones were identified by

Southern blot. Two positives clones exhibiting a normal karyotype were used to generate chimeric mice by microinjection into C57BL/6 blastocysts. Germline transmission of the targeted allele was confirmed by Southern blot analysis of tail DNA from the agouti offspring.

T2/Onc excision PCR

Genomic DNAs were obtained from *Pdx1-cre; T2/Onc; Rosa26-LSL-SB13* (CTSB13) and *T2/Onc; Rosa26-LSL-SB13* (TSB13) mice and primers used to assess the excision of the T2/Onc concatemer in the CTSB13 mice were: 5'-TGTGCTGCAAGGCGATTA-3' and 5'-ACCATGATTACGCCAAGC-3'.

CIS analysis

For the statistical analysis, 90,007 non-redundant insertion sites (Supplementary Table 3) were used to identify CISs using a Gaussian Kernel Convolution framework (GKC)²⁸. An enhanced version of the framework was developed for SB screens to account for the local density of TA sites within the genome²⁵. For example, a genomic region containing a large number of insertion sites but a low density of TA sites is considered to be significant and thereby identified as a candidate CIS. Conversely, a region with a large number of insertion sites but also containing a high density of TA sites is determined to be less significant, since the transposons have more “target” sites into which they can integrate. Multiple kernel scales were employed in the GKC framework (widths of 15K, 30K, 50K, 75K, 120K and 240K nucleotides). CISs predicted across multiple scales and overlapping in their genomic locations were clustered together, such that the CIS with the smallest genomic “footprint” was reported as the representative CIS. For highly significant CISs with narrow spatial distributions of insertion sites, the 15K kernel is typically the scale on which CISs are identified. Additional statistical analysis of insertion sites was performed using a Monte Carlo framework¹⁰. CISs were compared to previously published datasets of human pancreatic cancer genetics^{5,29,30}.

Detection of *Usp9x-T2/Onc* fusion mRNA by RT-PCR in SB tumors

Total RNA was extracted from snap-frozen SB tumors using the RNeasy Mini Kit (Qiagen), and total RNA (1 µg) was reverse transcribed into cDNA using the High Capacity RNA-to-cDNA Kit (Applied Biosystems). RT-PCR was carried out with a nested PCR approach using primers of mouse *Usp9x* exon 1 and the Carp-β-Actin splice acceptor sequence of the T2/Onc transposon cassette. cDNA was used as a template in a first round of PCR using specific primers corresponding to exon 1 of *Usp9x* (5-gagtctgcgctgccgctgctg-3') and Carp-β-Actin splice acceptor sequence (5'-cataccggctactgtgctaa-3'). The product of this reaction was used as a template in a second round of nested PCR using an internal primer in the *Usp9x* exon 1 (5'-gctgccgctgctgttctgctg-3') and a second primer in the Carp-β-Actin splice acceptor sequence (5'-acgttgctaaccaaccagtgc-3'). PCR products were cloned into pCR 2.1-TOPO vector (Invitrogen) and positives clones sequenced.

Plasmids, shRNAs and transfections

pSuperRetro-PURO retroviral vector (Oligoengine) expressed a short hairpin against mouse and human *USP9x* (5'-gatgaggaacctgcattc-3'), mouse *Itch* (5'-gacctgagaagacgtttgt-3')³¹, and a scramble sequence (5'-gcgcgctttgtaggattcg-3'). pBabe-zeo-Ecotropic Receptor (ecoR) was obtained from Addgene (plasmid#10687). Myc-mItch cDNA was released from pCINeo-myc-Itch (Addgene plasmid#11427), and was subcloned in the retroviral vector pBabe-neo (Addgene plasmid#1767). KCU1 and KCU2 cell lines were transfected with pEF-DEST51-mUsp9x(WT)-V5 and pEF-DEST51-mUsp9x(C1566S)-V5 plasmids^{32,33}. The plasmid pEF/GW-51/LacZ (Invitrogen) was used as control. Transfections were done using Lipofectamine 2000 (Invitrogen). 24 hours later, cells were selected with 5 µg/ml blasticidin (Invitrogen).

Cell culture

Tumor pancreatic cancer cell lines were established from *Kras^{LSL-G12D}; Pdx1-cre* (T4878 and T9394), *Kras^{LSL-G12D}; P48-cre* (TB1572) and *Kras^{LSL-G12D}; Pdx-1-Cre; Usp9x^{fl}* (KCU1 and KCU2) mice as described previously³⁴. Cells were subsequently cultured in DMEM (Invitrogen), supplemented with 10% FCS (Hyclone). The normal human pancreatic ductal cell line HPDE was generously provided by Dr. Tsao and cultured as described previously^{35,36}. The human pancreatic cancer cell lines AsPC1 (CRL-1682) and BxPC3 (CRL-1687) were acquired from ATCC and cultured according to instructions. The other cell lines were obtained from Clare Hall Laboratories (CRUK). The human cell lines Panc1, MiaPaCa2, 818.4, Hs766T, PATU2, SUIT2, FA6 and MDA-Panc3 (PDA); CaCO2 and SW1116 (colorectal cancer); SKBR3 (breast cancer) and A549 (lung cancer) were cultured in DMEM supplemented with 10% FCS. The human cell lines U937 (histiocytic lymphoma); RAMOS (Burkitt's lymphoma); NCI-H2179 (lung cancer) and ZR75-1 (breast cancer) were cultured in RPMI (Invitrogen) supplemented with 10% FCS. Cells were treated with 1 µM trichostatin A (Sigma) for 24 hours or with 5 µM 5-Aza-2'-deoxycytidine (Sigma) for 96 hours where indicated to obtain RNA and protein lysates to assess USP9x expression. For anchorage-independent growth assay, cells were treated with 5 µM 5-Aza-2'-deoxycytidine (Sigma).

Retroviral infections

Phoenix cells were plated 24 hr before transfection using the ProFection Mammalian Transfection System Calcium Phosphate (Promega). Target cells were infected with retroviruses produced in the Phoenix packaging cells (24 and 48 hr after transfection) in the presence of 8 µg/ml polybrene (Sigma) and were selected with 2 µg/ml puromycin (Sigma) or 1 mg/ml G418 (Clontech). Experiments were performed using at least 2 independent cell line infected pools. Human PDA cells lines Panc1, SUIT2 and PATU2 infected with retroviral vectors expressed the Ecotropic Receptor (ecoR).

Transformation, Anoikis and EMT assays

Cell lines (1.5×10^4 cells) were plated in triplicate in 12-well plates and counted as indicated using a Z2 Coulter (Beckman). Cells were fed every other day. Anchorage-independent growth assay was assessed by colony formation in soft agar. Briefly, 15,000 cells were

plated in duplicates in DMEM with 15% serum and 0.34% low-melting point agarose (LMP, BioGene) onto 6-cm dishes coated with 0.5% LMP. Cells were fed twice a week and grown for 2 weeks. For the anoikis assay, 10^5 cells/0.5 ml were plated in 24 well ultra low cluster plates (Costar) to allow them to grow in suspension for 4 days. Cells were harvested, washed with cold PBS and protein lysates were obtained. Cell line T4878 was cultured in matrigel as previously described³⁷, plating 1000 cells/well. Cells were fed every 2 days and grown for 4 days. Epithelial-to-Mesenchymal Transition (EMT) was determined by plating 10^5 cells/6 well plates for 24 hr to allow attachment, followed by treatment with human TGF- β 1 (5 ng/ml) (RD Systems) for 24 hr. p21 induction was assessed after treatment with human TGF- β 1 (5 ng/ml) (RD Systems) for 2 hr.

Real-time PCR

Total RNA from human PDA cell lines was extracted using the Rneasy Mini Kit (Qiagen), and total RNA (1 μ g) was reverse transcribed into cDNA using the High Capacity RNA-to-cDNA kit (Applied Biosystems). Human *USP9x* expression was analyzed by quantitative PCR (q-PCR) using TaqMan gene expression assays Hs00245009_m1 (Applied Biosystems) on a 7900HT Real-Time PCR system (Applied Biosystems). Gene expression was normalized to human β -*ACTIN* expression, assessed with the gene expression assays Hs99999903_m1 (Applied Biosystems), and shown relative to control samples.

Western blot analysis

Cells were washed three times in cold PBS and lysed with boiling lysis buffer (1% SDS; 10mM, pH 7.5 Tris; 50mM NaF; 1mM Na_3VO_4). Lysates were boiled 5 minutes, passed through a 26 gauge needle to shear genomic DNA and centrifuged for 10 minutes at 14,000 rpm. Equivalent amounts of protein were resolved in 4–12% gradient SDS-PAGE gels (Invitrogen), transferred to Immobilon-P Transfer Membranes (Millipore), and incubated with the corresponding antibodies including anti-Ask1 (NB110-55482, Novus Biologicals); anti-Mcl1 (5453, Cell Signaling); anti-Usp9x (A301-351A, Bethyl); anti-CC3 (9664, Cell Signaling); anti-Itch (611198, BD); anti-p21 (sc-6246, Santa Cruz); anti-Smad4 (sc-7966, Santa Cruz); anti-myc tag (2276, Cell Signaling); anti V5 tag (R960-25, Invitrogen); anti-c-FLIP (ALX-804-127, Enzo Life Sciences); anti-c-Jun (9165, Cell Signalling); anti-p63 (Ab110038, Abcam); anti α -Tubulin (T6074, Sigma) and anti-Actin (sc-1616, Santa Cruz Biotechnology). Reactive bands were visualized with ECL plus reagent (Amersham). Relative expression was quantified with Image Quant TL software (GE Healthcare)

Immunohistochemistry

Formalin-fixed paraffin-embedded (FFPE) mouse tissues were cut into 3- μ m tissue sections, and antigen retrieval was performed in 10mM, pH 6.0 citric acid (for Usp9x and E-cadherin) or 10mM, pH 8.0 EDTA (for Smad4). Endogenous peroxidases were quenched in 3% H_2O_2 /PBS for 20 minutes. Signal detection for immunohistochemistry was accomplished with biotinylated secondary antibodies (Vector Laboratories, Burlingame, CA) using the Elite Vectastain ABC kit and peroxidase substrate DAB kit (Vector Laboratories, Burlingame, CA). Primary antibodies used were anti-Usp9x, 1:200 (A301-351A, Bethyl); E-

cadherin, 1:200 (610182, BD) and anti-Smad4, 1:100 (sc-7966, Santa Cruz). Slides were counterstained with hematoxylin.

Clinical patient samples immunohistochemistry and analysis

Tissue microarrays (n=404) were prepared from patient samples obtained after appropriate informed consent in Dresden (Institute of Pathology, University Hospital Dresden), Regensburg (Institute of Pathology, University Hospital Regensburg) and Jena (Institute of Pathology, University Hospital Jena). Informed consent was obtained for each patient, following review by the human ethics committee Ethikkommission an der Technischen Universität Dresden. The PDA tumor samples were collected from 1993–2009, and the majority of the patients (65%) did not undergo adjuvant chemotherapy. Those that did undergo adjuvant therapy (35%) were chiefly treated with 5FU or gemcitabine-based regimens, but in this subgroup there was no significant increase in patient survival. The median survival times of patients following surgery from each center were indistinguishable. Immunohistochemistry was performed on 5 µm sections that were prepared using silanized slides (Menzel Gläser, Braunschweig, Germany). Staining was performed with the Benchmark System (Ventana, Illkirch, France), using rabbit anti-USP9X antibody, 1:200 (A301-351A, Bethyl) and anti-ITCH, 1:200 (611198, BD); and the protocol UltraView HRP, with the CC1 modified protocol as pretreatment. Slides were counterstained with hematoxylin. Staining intensities were scored as absent (0), weak (1), medium (2) and strong (3). For further analysis the staining intensities were grouped as negative (0) and positive (1–3). The Cox regression model assumption of proportional hazard was tested using a plot of the cumulative hazards function.

A second cohort of patient samples was obtained from the Gastrointestinal Cancer Rapid Medical Donation Program in the Department of Pathology at Johns Hopkins Hospital, USA. Use of all human tissue samples from resection specimens and autopsy participants was approved by Johns Hopkins Institutional Review Board, and obtained after informed consent. All samples were collected within 12 hours postmortem and formalin fixed before paraffin embedding. 5 µm sections were cut from matched primary and metastasis samples onto glass slides. Slides were first incubated in Dako Target Retrieval Solution for antigen retrieval. Slides were then incubated with rabbit anti-USP9X antibody, 1:1000 (ab26334, Abcam) or 1:200 (NBP1-48321, Novus Biologicals), and anti-SMAD4 as previously described³⁸. Signal detection for immunohistochemistry was accomplished with Dako LSAB+System-HRP. Slides were counterstained with hematoxylin.

An additional cohort of pancreatic cancer resection samples was prospectively acquired through the Australian Pancreatic Cancer Network and the Australian Pancreatic Cancer Genome Initiative (<http://www.pancreaticcancer.net.au/apgi>). Consent was obtained for genomic sequencing through the Australian Pancreatic Cancer Genome Initiative (APGI) for each individual patient following approval from Human Research Ethics Committees (HREC) at participating sites (Sydney South West Area Health Service HREC Western Zone, 2006/054; Sydney Local Health Network HREC RPA Zone, X11-0220 and North Sydney Central Coast Health, Harbour HREC, 0612-251M). We extracted RNA from tumour samples using the Qiagen Allprep[®] Kit (Qiagen, Valencia, CA) in accordance with

the manufacturer's instructions, assayed for quality on an Agilent Bioanalyzer 2100 (Agilent Technologies, Palo Alto, CA), and subsequently hybridized to Illumina Human HT-12 V4 microarrays. Raw idat files were processed using *IlluminaGeneExpressionIdatReader* (Cowley *et al.* manuscript in preparation). Following array quality control, these data were vs.t transformed, and then robust spline normalized, using the *lumi* R/Bioconductor package. For the ICGC-APGI cohort, we assumed a proportional hazard: that the probability of death is the same for those censored as for those remaining on study.

For the TMA and expression array cohorts, median survival was estimated using the Kaplan-Meier method and the difference was tested using the log-rank test. P-values of less than 0.05 were considered statistically significant. For the TMA cohort, as few parameters were significant in univariate analysis, all were initially considered for Cox Proportional Hazard multivariate analysis in a backward elimination model, and assessed with the SPSS18 Software (IBM, Ehningen, Germany) with overall survival used as the primary endpoint. For the ICGC-APGI cohort, clinico-pathologic variables analyzed with a P-value of less than 0.25 on log-rank test were entered into Cox Proportional Hazard multivariate analysis and the model was resolved using backward elimination. Statistical analysis was performed using StatView 5.0 Software (Abacus Systems, Berkeley, CA, USA). Disease-specific survival was used as the primary endpoint.

Supplementary Material

Refer to Web version on PubMed Central for supplementary material.

Acknowledgments

We thank Patricia Labosky for assistance in generating the *Rosa26-LSL-SB13* mouse, B. Bhagavan for pathology consultation, Ming Tsao for kindly providing the HPDE cell line, and Neal Copeland and Karen Mann for sharing pre-published information. We thank Aarthi Gopinathan, Herve Tiriac, Danielle Engle, Derek Chan, Frances Connor, Sahra Derkits and other members of the Tuveson lab for assistance and advice, and the animal care staff and histology core at CRI, and The University of Minnesota's Mouse Genetics Laboratory. This research was supported by the University of Cambridge and Cancer Research UK, The Li Ka Shing Foundation and Hutchison Whampoa Limited, the NIHR Cambridge Biomedical Research Centre, and the NIH (2P50CA101955 SPORE grant to DAT, DAL, CAI-D; grants CA62924, CA128920 and CA106610 to CAI-D; P50CA62924 SPORE grant to RHH and CAI-D; and CA122183 to LSC). DJA is supported by Cancer Research UK and the Wellcome Trust. LvdW is supported by the Kay Kendall Leukemia Fund. CP is supported by Wilhelm Sander Stiftung (2009.039.1) and DFG (PI 341/5-1). AVB, DKC, SMG and the APGI investigators are funded by the National Health and Medical research Council of Australia (NHMRC); Queensland Government; Cancer Council NSW; Australian Cancer Research Foundation; Cancer Institute NSW; The Avner Nahmani Pancreatic Cancer Research Foundation; and the R.T. Hall Trust. Additional support was obtained from Fundación Ibercaja (PAP-M). We regret that many primary references have been omitted due to space limitations.

References

1. Almoguera C, et al. Most human carcinomas of the exocrine pancreas contain mutant c-K-ras genes. *Cell*. 1988; 53:549–554. [PubMed: 2453289]
2. Caldas C, et al. Frequent somatic mutations and homozygous deletions of the p16 (MTS1) gene in pancreatic adenocarcinoma. *Nat Genet*. 1994; 8:27–32. [PubMed: 7726912]
3. Redston MS, et al. p53 mutations in pancreatic carcinoma and evidence of common involvement of homocopolymer tracts in DNA microdeletions. *Cancer Res*. 1994; 54:3025–3033. [PubMed: 8187092]
4. Hahn SA, et al. DPC4, a candidate tumor suppressor gene at human chromosome 18q21.1. *Science*. 1996; 271:350–353. [PubMed: 8553070]

5. Jones S, et al. Core signaling pathways in human pancreatic cancers revealed by global genomic analyses. *Science*. 2008; 321:1801–1806. [PubMed: 18772397]
6. Collier LS, Carlson CM, Ravimohan S, Dupuy AJ, Largaespada DA. Cancer gene discovery in solid tumours using transposon-based somatic mutagenesis in the mouse. *Nature*. 2005; 436:272–276. [PubMed: 16015333]
7. Dupuy AJ, Akagi K, Largaespada DA, Copeland NG, Jenkins NA. Mammalian mutagenesis using a highly mobile somatic Sleeping Beauty transposon system. *Nature*. 2005; 436:221–226. [PubMed: 16015321]
8. Hingorani SR, et al. Preinvasive and invasive ductal pancreatic cancer and its early detection in the mouse. *Cancer cell*. 2003; 4:437–450. [PubMed: 14706336]
9. Schwickart M, et al. Deubiquitinase USP9X stabilizes MCL1 and promotes tumour cell survival. *Nature*. 2010; 463:103–107. [PubMed: 20023629]
10. Keng VW, et al. A conditional transposon-based insertional mutagenesis screen for genes associated with mouse hepatocellular carcinoma. *Nat Biotechnol*. 2009; 27:264–274. [PubMed: 19234449]
11. Starr TK, et al. A transposon-based genetic screen in mice identifies genes altered in colorectal cancer. *Science*. 2009; 323:1747–1750. [PubMed: 19251594]
12. Collier LS, et al. Whole-body sleeping beauty mutagenesis can cause penetrant leukemia/lymphoma and rare high-grade glioma without associated embryonic lethality. *Cancer Res*. 2009; 69:8429–8437. [PubMed: 19843846]
13. Avizienyte E, et al. LKB1 somatic mutations in sporadic tumors. *Am J Pathol*. 1999; 154:677–681. [PubMed: 10079245]
14. Varela I, et al. Exome sequencing identifies frequent mutation of the SWI/SNF complex gene PBRM1 in renal carcinoma. *Nature*. 2011; 469:539–542. [PubMed: 21248752]
15. Su GH, et al. ACVR1B (ALK4, activin receptor type 1B) gene mutations in pancreatic carcinoma. *Proc Natl Acad Sci U S A*. 2001; 98:3254–3257. [PubMed: 11248065]
16. Li M, et al. Deubiquitination of p53 by HAUSP is an important pathway for p53 stabilization. *Nature*. 2002; 416:648–653. [PubMed: 11923872]
17. Dupont S, et al. FAM/USP9x, a deubiquitinating enzyme essential for TGFbeta signaling, controls Smad4 monoubiquitination. *Cell*. 2009; 136:123–135. [PubMed: 19135894]
18. Nagai H, et al. Ubiquitin-like sequence in ASK1 plays critical roles in the recognition and stabilization by USP9X and oxidative stress-induced cell death. *Mol Cell*. 2009; 36:805–818. [PubMed: 20005844]
19. Sun H, et al. Bcr-Abl ubiquitination and Usp9x inhibition block kinase signaling and promote CML cell apoptosis. *Blood*. 2011; 117:3151–3162. [PubMed: 21248063]
20. Mouchantaf R, et al. The ubiquitin ligase itch is auto-ubiquitylated in vivo and in vitro but is protected from degradation by interacting with the deubiquitylating enzyme FAM/USP9X. *J Biol Chem*. 2006; 281:38738–38747. [PubMed: 17038327]
21. Bernassola F, Karin M, Ciechanover A, Melino G. The HECT family of E3 ubiquitin ligases: multiple players in cancer development. *Cancer cell*. 2008; 14:10–21. [PubMed: 18598940]
22. Wang X, Soloway PD, Clark AG. Paternally biased X inactivation in mouse neonatal brain. *Genome Biol*. 2010; 11:R79. [PubMed: 20663224]
23. Yang F, Babak T, Shendure J, Disteche CM. Global survey of escape from X inactivation by RNA-sequencing in mouse. *Genome Res*. 2010; 20:614–622. [PubMed: 20363980]
24. Jackson EL, et al. Analysis of lung tumor initiation and progression using conditional expression of oncogenic K-ras. *Genes Dev*. 2001; 15:3243–3248. [PubMed: 11751630]
25. March HN, et al. Insertional mutagenesis identifies multiple networks of cooperating genes driving intestinal tumorigenesis. *Nature genetics*. 2011; 43:1202–1209. [PubMed: 22057237]
26. Uren AG, et al. A high-throughput splinkerette-PCR method for the isolation and sequencing of retroviral insertion sites. *Nature protocols*. 2009; 4:789–798. [PubMed: 19528954]
27. Tompers DM, Labosky PA. Electroporation of murine embryonic stem cells: a step-by-step guide. *Stem Cells*. 2004; 22:243–249. [PubMed: 15153600]

28. de Ridder J, Uren A, Kool J, Reinders M, Wessels L. Detecting statistically significant common insertion sites in retroviral insertional mutagenesis screens. *PLoS Comput Biol*. 2006; 2:e166. [PubMed: 17154714]
29. Grutzmann R, et al. Gene expression profiling of microdissected pancreatic ductal carcinomas using high-density DNA microarrays. *Neoplasia*. 2004; 6:611–622. [PubMed: 15548371]
30. Pilarsky C, et al. Activation of Wnt signalling in stroma from pancreatic cancer identified by gene expression profiling. *J Cell Mol Med*. 2008; 12:2823–2835. [PubMed: 18298655]
31. Oberdoerffer P, et al. Efficiency of RNA interference in the mouse hematopoietic system varies between cell types and developmental stages. *Mol Cell Biol*. 2005; 25:3896–3905. [PubMed: 15870264]
32. Nathan JA, et al. The ubiquitin E3 ligase MARCH7 is differentially regulated by the deubiquitylating enzymes USP7 and USP9X. *Traffic*. 2008; 9:1130–1145. [PubMed: 18410486]
33. Murray RZ, Jolly LA, Wood SA. The FAM deubiquitylating enzyme localizes to multiple points of protein trafficking in epithelia, where it associates with E-cadherin and beta-catenin. *Mol Biol Cell*. 2004; 15:1591–1599. [PubMed: 14742711]
34. Olive KP, et al. Inhibition of Hedgehog signaling enhances delivery of chemotherapy in a mouse model of pancreatic cancer. *Science*. 2009; 324:1457–1461. [PubMed: 19460966]
35. Ouyang H, et al. Immortal human pancreatic duct epithelial cell lines with near normal genotype and phenotype. *Am J Pathol*. 2000; 157:1623–1631. [PubMed: 11073822]
36. Furukawa T, et al. Long-term culture and immortalization of epithelial cells from normal adult human pancreatic ducts transfected by the E6E7 gene of human papilloma virus 16. *Am J Pathol*. 1996; 148:1763–1770. [PubMed: 8669463]
37. Debnath J, Muthuswamy SK, Brugge JS. Morphogenesis and oncogenesis of MCF-10A mammary epithelial acini grown in three-dimensional basement membrane cultures. *Methods*. 2003; 30:256–268. [PubMed: 12798140]
38. Iacobuzio-Donahue CA, et al. DPC4 gene status of the primary carcinoma correlates with patterns of failure in patients with pancreatic cancer. *J Clin Oncol*. 2009; 27:1806–1813. [PubMed: 19273710]

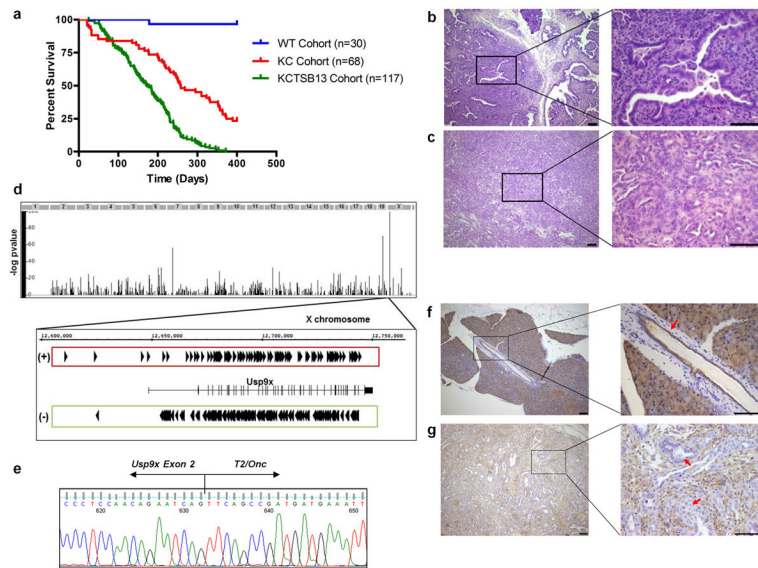


Figure 1. Transposon mutagenesis accelerates murine PDA and targets *Usp9x*
a. Increased mortality of KCTSB13 mice compared to KC cohort (containing KCT, KCSB13 and KC mice) (172 vs. 257 days, $p < 0.001$; long-rank test). Wild-type (WT) cohort is comprised of KTSB13 and CTSB13 mice. **b–c.** Invasive cystic neoplasm (**b**), and mPDA (**c**) in KCTSB13 mice. Scale bar: 100 μ m. **d.** *Usp9x* is the major CIS in KCTSB13 PDA tumors (X-axis denotes genome, Y-axis $-\log$ P-value), with bidirectional insertions. (+) parallel to *Usp9x* expression, (–) antiparallel. **e.** *Usp9x* Exon 2-*T2/Onc* chimeric mRNA in SB13 tumors. **f–g.** *Usp9x* protein expression in normal pancreatic ducts (arrow) (**f**), but not in neoplastic cells (**g**) (arrows) in SB13 PDA harboring *Usp9x* insertions. Scale bar: 100 μ m.

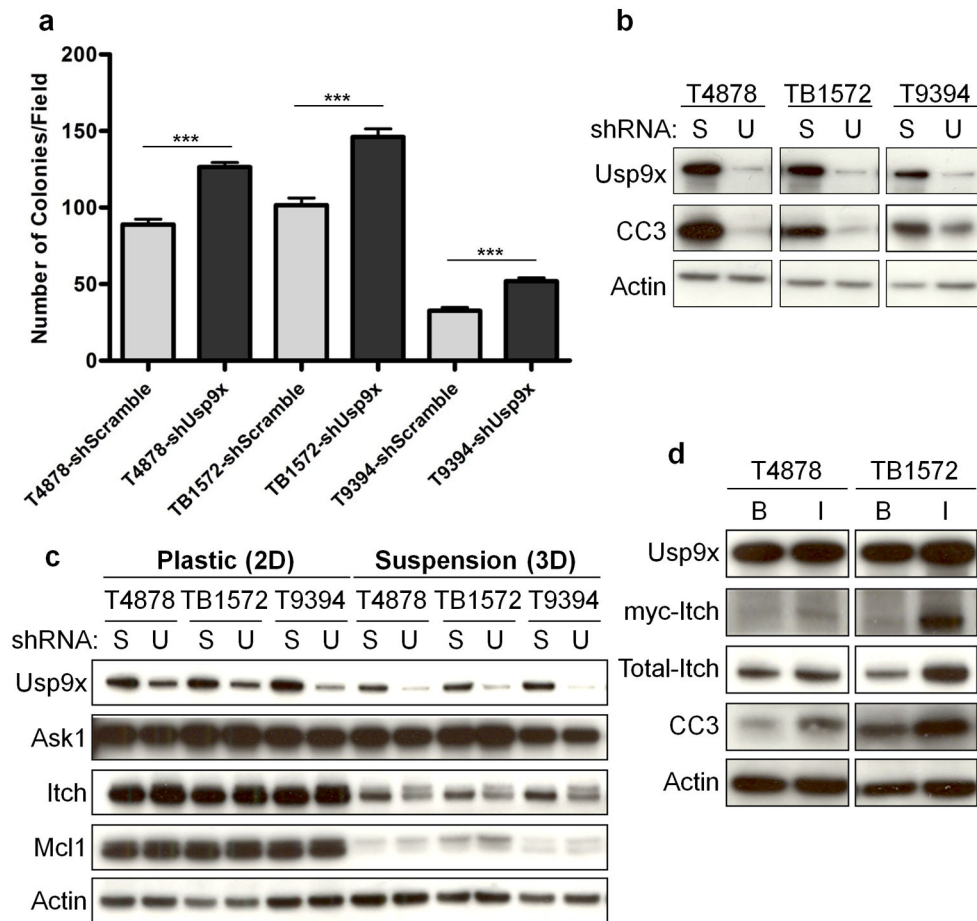


Figure 2. Usp9x regulates PDA cellular transformation and Itch

a–b, Usp9x knock-down promotes anchorage-independent growth in three mPDA cell lines (**a**), and decreases anoikis denoted by cleaved caspase 3 (CC3) (**b**). The mean and s.e.m. of one representative experiment performed in triplicate are shown in (**a**) (***, $p < 0.001$; Mann Whitney test). (S: Scramble; U: Usp9x). **c**, Usp9x knock-down decreases Itch but not Ask1 or Mcl1. Changes in Itch are more evident in suspension cultures, and the slower migrating band has the expected mobility of mono-ubiquitinated Itch. **d**, Ectopic Itch induces anoikis. (B: pBabe-neo; I: pBabe-neo-myc-Itch).

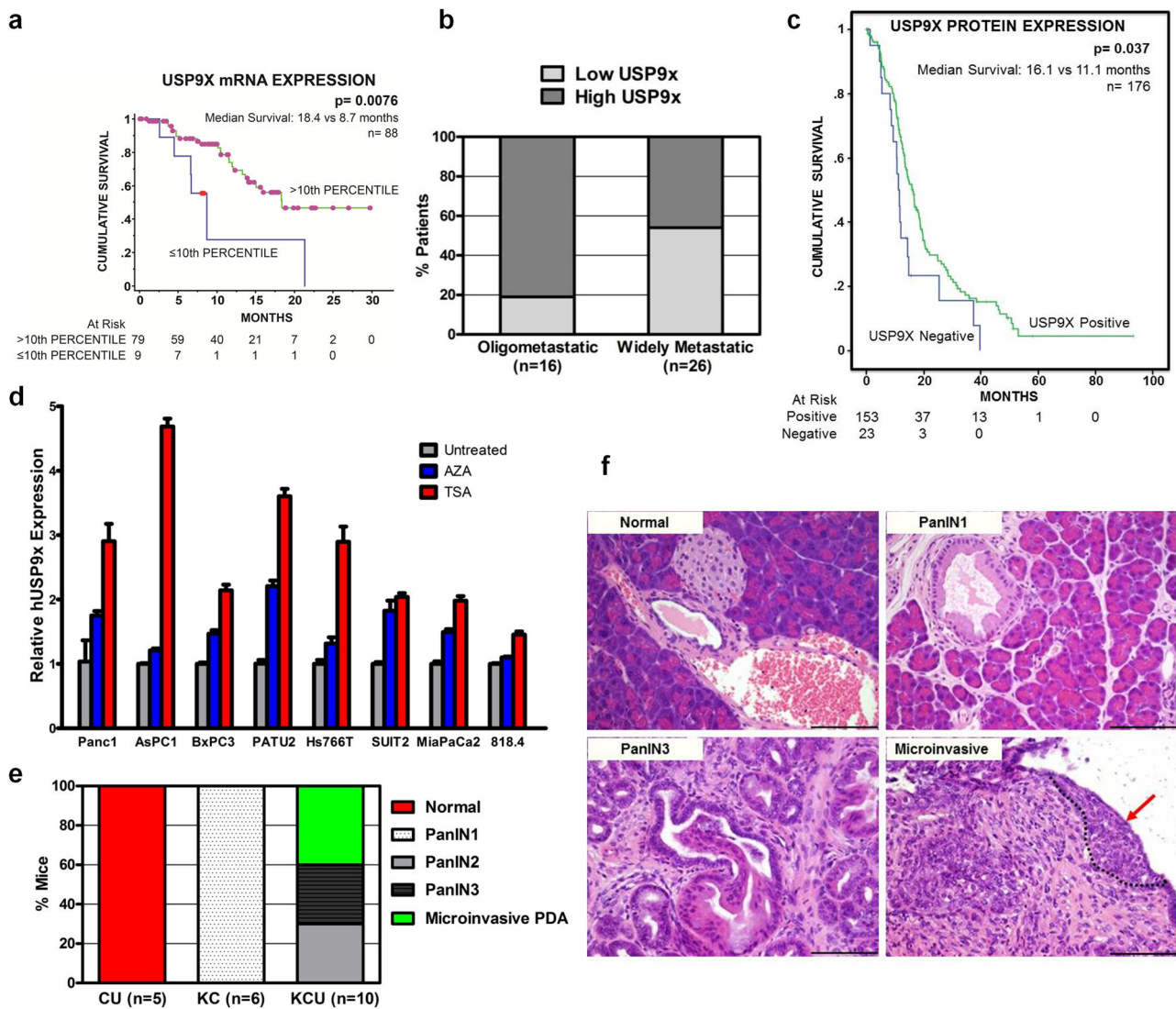


Figure 3. *USP9X* loss promotes PDA

a–c, Decreased *USP9X* expression correlates with shortened survival in Australian post-surgical cohort (**a**) (8.7 vs. 18.4 months, $p=0.0076$; log-rank test), increased metastatic burden in American autopsy series (**b**) (54% vs. 19%, $p=0.0212$; Fisher’s exact test), and diminished survival in German post-surgical cohort (**c**) (11.1 vs. 16.1 months, $p=0.037$; log-rank test). **d**, Trichostatin A (TSA, Red) and 5-Aza-2'-deoxycytidine (AZA, Blue) modestly increase *USP9X* mRNA expression. The mean and s.e.m. of one representative experiment performed in triplicate are shown. **e**, *Usp9x* deletion promotes mPanIN progression in KCU mice ($p<0.0001$; Fisher’s exact test). **f**, Representative normal pancreas (CU), mPanIN1 (KC), mPanIN3 (KCU) and microinvasive mPDA (KCU, arrow, circled). Scale bar: 100 μ m.

Table 1
Top 20 candidate genes that cooperate with *Kras^{G12D}* to promote mPDA in KCTS13 mice

CISs were scored by tumor frequency with the narrowest 15K kernel spatial distribution of insertion sites. Chr: chromosome; N: number of tumors from which the CIS was found; I, total number of insertions of the CIS in the indicated tumors.

Gene	Chr	CIS Peak Location	CIS Height	N	I	Mutation in humans
Usp9x	X	12691773	158.1266	101	341	
Pten	19	32872602	64.5204	61	96	
Fndc3b	3	27562591	13.7096	55	67	
Setd5	6	113057997	35.6176	52	71	
Arrip1 Fbxw7	3	84769635	21.6666	48	80	Yes ⁵
Fam193a	5	34705809	24.3555	45	78	
Cttna1	18	35342868	20.2017	45	50	
Magil1	6	93859940	13.3715	43	57	
Mkin1	6	31414109	16.5263	41	53	
Pum1	4	130288478	12.7948	41	46	Yes ⁵
Farp1	14	121587858	9.407	39	47	
Foxp1	6	98921646	19.5831	38	60	
Arid1a	4	133268936	32.1628	38	47	Yes ⁵
Acvr1b	15	101024934	31.1752	38	47	Yes ¹⁵
Map4k3	17	81109860	13.2385	38	45	Yes ⁵
Stag2	X	39535994	16.8613	37	48	
Mll5	5	22982314	16.0001	37	43	Yes ⁵
Atxn2 Sh2b3	5	122267680	12.3174	37	41	
Arhgap5	12	53644560	37.416	35	61	
Gsk3b	16	38106972	21.79	35	43	